Cylindrical Bragg mirrors on leg segments of the male Bolivian blueleg tarantula *Pamphobeteus antinous* (Theraphosidae)

Priscilla Simonis,* Annick Bay, Victoria L. Welch, Jean-François Colomer, and Jean Pol Vigneron

Research Center in Physics of Matter and Radiation (PMR), University of Namur (FUNDP), rue de Bruxelles, 61, B-5000 Namur Belgium

**priscilla.simonis@fundp.ac.be*

Abstract: The large male tarantula *Pamphobeteus antinous* is easily recognized at the presence of blue-violet iridescent bristles on some of the segments of its legs and pedipalps. The optical properties of these colored appendages have been measured and the internal geometrical structure of the bristles have been investigated. The coloration is shown to be caused by a curved coaxial multilayer which acts as a "cylindrical Bragg mirror".

OCIS codes: (330.0330) Vision, color, and visual optics; (170.1420) Biology; (050.5298) Photonic crystals; (060.4005) Microstructured fibers; (230.4170) Multilayers.

References and links

1. M. F. Land, J. Horwood, M. L. M. Lim, and D. Li, "Optics of the ultraviolet reflecting scales of a jumping spider," Proc. Roy. Soc. B **274,** 1583–1589 (2007).
2. A. L. Ingram, A. D. Ball, A. R. Parker, O. Deparis, J. Boulenguez, and S. Berthier, "Characterization of the green iridescence on the chelicerae of the tube web spider, *Segestria florentina* (Rossi 1790) (Araneae, Segestriidae)," J. Arachnol. **37,** 68–71 (2009).
3. R. I. Pocock, "On some genera and species of South American Avicullariidae," Ann. Mag. nat. Hist. **11**(7), 81–115 (1903).
4. R. G. Breene, D. A. Dean, J. C. Cokendolpher, and B. H. Reger, "Tarantulas of Texas: Their medical importance, and world-wide bibliography to the Theraphosidae (Araneae)," (American Tarantula Society, South Padre Island, Texas,1996).
5. R. Bertani, C. S. Fukushima, and P. I. da Silva Júnior, "Two new species of Pamphobeteus Pocock, 1901 (Araneae: Mygalomorphae: Theraphosidae) from Brazil, with a new type of stridulatory organ," Zootaxa **1826,** 45–58 (2008).
6. D. M. Teixeira, G. Luigi and I. M. Schloemp, "Aves brasileiras como presas de artropodes," Ararajuba **2,** 69–74 (1991).
7. H. Ghiradella, "Insect cuticular surface modifications: scales and other structural formations," in *Advances in Insect Physiology*, Jérôme Casas and Stephen J. Simpson, ed. **38,** (Academic Press, Burlington, 2010), 136–180.
8. M. F. Land, "The physics and biology of animal reflectors," Prog. Biophys. Mol. Biol. **24,** 75106 (1972).
9. A. R. Parker, D. R. Mc Kenzie, and M. C. J. Large, "Multilayer reflectors in animals using green and gold beetles as contrasting examples," J. Exp. Biol. **201,** 1307–1313 (1998).
10. M. Srinivasarao, "Nano-optics in the biological world: beetles, butterflies, birds and moths," Chem. Rev. **99**(7), 1935–1962 (1999).
11. P. Vukusic and J. R. Sambles, "Photonic structures in biology," Nature **424,** 852–855 (2003).
12. S. Kinoshita, S. Yoshioka, and J. Miyazaki, "Physics of structural colors," Rep. Prog. Phys. **71,** 076401 (2008).
13. A. E. Seago, P. Brady, J. P. Vigneron, and T. D. Schultz, "Gold bugs and beyond: a review of iridescence and structural colour mechanisms in beetles (Coleoptera)," J. R. Soc. Interf. **6**(Suppl. 2), S165–S184 (2009).

#183854 - $15.00 USD Received 22 Jan 2013; revised 23 Feb 2013; accepted 23 Feb 2013; published 13 Mar 2013

14. L. P. Biró and J. P. Vigneron, "Photonic nanoarchitectures in butterflies and beetles: valuable sources for bioinspiration," Laser & Phot. Rev. **5,** 27–51 (2011).
15. A. C. Neville and S. Caveney, "Scarabeid beetle exocuticle as an optical analogue of cholesteric liquid crystals," Biol. Rev. **44,** 531–562 (1969).
16. A. R. Parker and D. R. McKenzie, "The cause of 50 million-year-old colour," Proc. Roy. Soc. Lond. B **270 (Suppl 2),** S151–S153 (2003).
17. M. Rassart, P. Simonis, A. Bay, O. Deparis, and J. P. Vigneron, "Scale coloration change following water absorption in the beetle Hoplia coerulea (Coleoptera)," Phys. Rev. E **80,** 031910 (2009).
18. E. R. Dufresne, H. Noh, V. Saranathan, S. G. J. Mochrie, H. Cao and R. O. Prum, "Self-assembly of amorphous biophotonic nanostructures by phase separation," Soft Matter **5,** 1792–1795 (2009).
19. S. Yoshioka and S. Kinoshita, "Direct determination of the refractive index of natural multilayer systems," Phys. Rev. E **83,** 051917 (2011).
20. P. Vukusic, "Quantified interference and diffraction in single Morpho butterfly scales," Proc. Roy. Soc. Lond. B **266 (1427),** 1403–1411 (1999).
21. J. P. Vigneron and V. Lousse, "Variation of a photonic crystal color with the Miller indices of the exposed surface," Proc. SPIE **6128,** 61281G1 (2006).
22. S. Kinoshita and S. Yoshioka, "Structural colors in nature: the role of regularity and irregularity in the structure," ChemPhysChem **6,** 1442–1459 (2005).
23. Lord Rayleigh, "On the reflection of light from a regularly stratified medium," Proc. Roy. Soc. Lond. A **93,** 565–577 (1917).
24. J. P. Vigneron and P. Simonis, "Structural colours," in *Advances in Insect Physiology*, Jérôme Casas and Stephen J. Simpson, ed. **38,** (Academic Press, Burlington, 2010), 181–218.
25. K. L. Kelly, "Color universal language and dictionary of names," (U.S. Department of Commerce, U.S.A.,1976).
26. C. F. Bohren and D. R. Huffman, *Absorption and Scattering of Light by Small Particles* (John Wiley and Sons, New York, 1983), pp. 194–219.
27. L. B. Evans, J. C. Chen and S. W. Churchill, "Scattering of electromagnetic radiation by infinitely long, hollow, and coated cylinders," J. Opt. Soc. Amer. **54 (8),** 1004–1007 (1964).
28. C. S. Kim and C. Yeh, "Scattering of an obliquely incident wave by a multilayered elliptical lossy dielectric cylinder," Radio Sci. **26**(5), 1165–1176 (1991).
29. E. Matijevic, R. H. Ottewill, and M. Kerker, "Light scattering by infinite cylinders, spider fibers," J. Opt. Soc. Amer. **51,** 115–116 (1960).
30. J. P. Vigneron, M. Ouedraogo, J.-F. Colomer, and M. Rassart, "Spectral sideband produced by a hemispherical concave multilayer on the African shield-bug *Calidea panaethiopica* (Scutelleridae)," Phys. Rev. E **79,** 021907 (2009).
31. A. Kienle and R. Hibst, "Light guiding in biological tissue due to scattering," Phys. Rev. Letters **97,** 018104 (2006).
32. A. F. Huxley, "A theoretical treatment of the reflexion of light by multilayer structures," J. Exp. Biol. **48,** 227–245 (1968).
33. O. Deparis, C. Vandenbem, M. Rassart, V. L. Welch, and J.-P. Vigneron, "Color-selecting reflectors inspired from biological periodic multilayer structures," Opt. Express **14 (8),** 3547–3555 (2006).
34. R. D. Dahl and A. M. Granda, "Spectral sensitivities of photoreceptor in the ocelli of the tarantula, Aphonopelma chalcodes (Araneae, Theraphosidae)," J. Arachnol. **17,** 195–205 (1989).
35. A. R. Parker, R. C. McPhedran, D. R. McKenzie, L. C. Botten, and N. A. Nicorovici, "Photonic engineering: Aphrodite's iridescence," Nature **409,** 36–37 (2001).
36. T. M. Trzeciak and P. Vukusic, "Photonic crystal fiber in the polychaete worm *Pherusa* sp.," Phys. Rev. E **80,** 061908 (2009).
37. D. G. Stavenga, M. A. Giraldo, and H. L. Leertouwer, "Butterfly wing colors: glass scales of *Graphium sarpedon* cause polarized iridescence and enhance blue/green pigment coloration of the wing membrane," J. Exp. Biol. **213,** 1731–1739 (2010).
38. J. P. Vigneron, P. Simonis, A. Aiello, A. Bay, D. M. Windsor, J.-F. Colomer, and M. Rassart, "Reverse color sequence in the diffraction of white light by the wing of the male butterfly *Pierella luna* (Nymphalidae: Satyrinae)," Phys. Rev. E **82,** 021903 (2010).
39. H. Ghiradella and M. Butler, "Many variations on a few themes: a broader look at iridescent scales (and feathers)," J. Roy. Soc. Interface **6,** S243–S251 (2009).
40. P. B. Clapham and M. C. Hutley, "Reduction of lens reflexion by the 'moth eye' principle," Nature **244,** 281–282 (1973).
41. J. P. Vigneron, M. Rassart, C. Vandenbem, V. Lousse, O. Deparis, L. P. Biró, D. Dedouaire, A. Cornet, and P. Defrance, "Spectral filtering of visible light by the cuticle of metallic woodboring beetles and microfabrication of a matching bioinspired material," Phys. Rev. E **73,** 041905 (2006).
42. D. P. Gaillot, O. Deparis, V. Welch, B. K. Wagner, J. P. Vigneron, and C. J. Summers, "Composite organic-inorganic butterfly scales: production of photonic structures with atomic layer deposition," Phys. Rev. E **78,** 031922 (2008).

#183854 - $15.00 USD Received 22 Jan 2013; revised 23 Feb 2013; accepted 23 Feb 2013; published 13 Mar 2013

43. H. Tabata, “Structurally colored fibers and applications,” in *Structural Colors in Biological Systems*, S. Kinoshita and S. Yoshioka, ed. (Osaka University Press, Osaka, Japan, 2005), 297–308.
44. C. E. Finlayson, C. Goddard, E. Papachristodoulou, D. R. E. Snoswell, A. Kontogeorgos, P. Spahn, G. P. Hellmann, O. Hess, and J. J. Baumberg, “Ordering in stretch-tunable polymeric opal fibers,” Opt. Express **19**(4), 3144–3154 (2011).

1. Introduction

Some spiders are known to have evolved photonic structures for coloration. Nearly perfect Bragg mirrors (i.e. dielectric multilayers) are found, for example, on jumping spiders [1] and tube-web spiders [2], resulting in brightly colored metallic-looking spots. In this work, we examine a different type of spider: a neotropical tarantula.

Tarantulas form a group of more than 800 species of spiders and are frequently large and hairy. All belong to the family Theraphosidae, which is one of fourteen families in the infraorder Mygalomorphae. Mygalomorphs are distinct from the so-called ”true” spiders (Araneomorphae) and differ in certain morphological details. These include the presence of patches of specialized bristles (called”scopulae”) in tarantulas that help with the adhesion of tarsi and metatarsi to the surface supporting the spider, or assist the functions of the tarsal claws.

Pamphobeteus antinous (Pocock, 1903) [3], under investigation here, is a very large tarantula originating from the southern neotropical region, essentially Peru and Bolivia. The mature male of this so-called ”Bolivian blueleg tarantula” displays, under specific illumination and viewing directions, a vivid blue-violet color on part of its dorsal side. The specimen examined in the present study was a mature male with a leg-span of 23 cm (see Fig. 1(a)).

2. The bristles: a versatile arthropod structure

Tarantulas have different types of bristles, which serve a variety of functions, including repelling water and making an efficient barrier to parasites. Some of their ”sensitive” setae are very specialized and many neotropical tarantulas, such as *Pamphobeteus antinous*, also bear urticating bristles and very rigid spines, that form part of a stridulation organ. The individual defence strategies of American tarantulas show several phases [4]. When not running away and hiding, a tarantula faces danger with a distinctive threat posture. If this fails, it makes intimidating forward movements and some tarantulas (like the one studied here) are able to produce a loud hissing sound from stridulatory organs [5]. Under a sustained threat, species possessing urticating bristles may deploy them defensively by rubbing off these bristles, which break close to their attachment point. The fine bristle-tips penetrate the opponent’s skin under a random direction and, because of the presence of rear-pointing barbs, progresses, producing further irritation. As far as has been observed, the discomfort is caused only by the structure of the bristle: no irritant chemical has been identified.

Some species of tarantulas are arboreal, but many more, like *Pamphobeteus antinous*, are terrestrial and typically live in burrows, from which they hunt prey. Large tarantulas need large prey, such as small rodents, lizards and birds [6] (Victorian biologists have introduced the vernacular name “birdeaters” for them). Mating is a complex process and the male first deposits sperm under a kind of silk cloth stretched on a natural wedged groove on the ground. He then calls for a receptive female: a process involving tapping the ground and taking expressive postures. The fact that the coloration studied here has only developed in mature adult males suggests that coloration and visual effects may also be part of the mating signals.

However, the coloration of the male *Pamphobeteus antinous* is not only interesting for its biological importance. The mechanism of coloration that will be explained in the next sections, has far-reaching and interesting consequences for the possibility of coloring fibers, including natural and artificial textile threads.

#183854 - $15.00 USD Received 22 Jan 2013; revised 23 Feb 2013; accepted 23 Feb 2013; published 13 Mar 2013

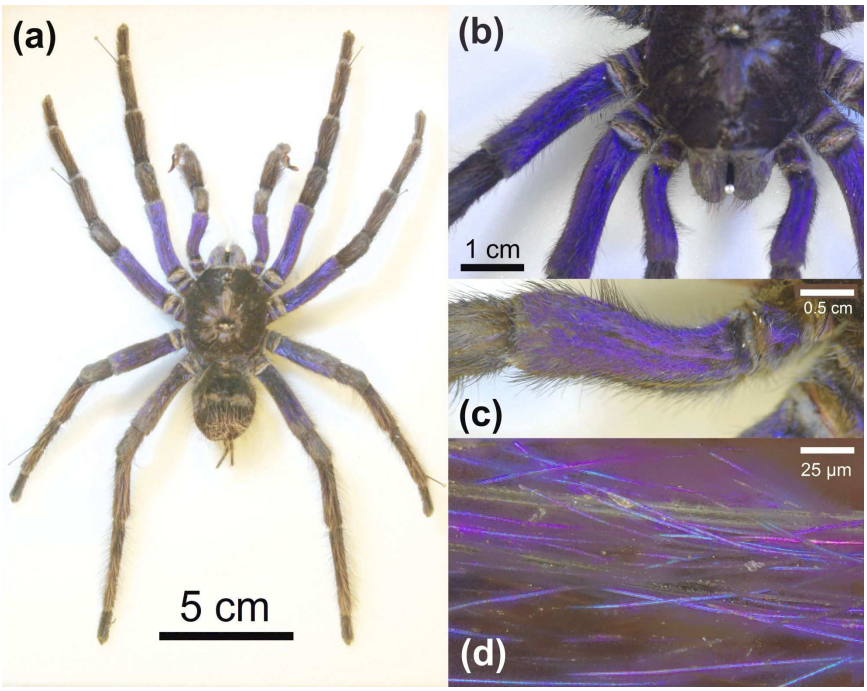

Fig. 1. (a) The male tarantula *Pamphobeteus antinous* displays a vivid violet-blue color on the three leg segments closest to its cephalothorax. (b) Blue areas on the dorsal side of the mature male *Pamphobeteus antinous*. Colored patches appear on the three inner segments of the legs and pedipalps, on the chelicerae and, less visible, on the dorsal cuticle of the thorax. The blue color originates from specialized bristles covering the cuticle. These bristles are roughly parallel, aligned along the length of the spider's leg segment. (c) Macrophotography of the bristles on the dorsal side of the pedipalp's femurs, oriented at a small angle to the symmetry plane of the body. (d) Optical microscope view of the blue setae, suggesting a roughly cylindrical shape. At this scale, individual setae are visible and a slight variation of color, from blue to violet is observable. Other, uncolored bristles also appear in the field.

3. Naked-eye perception and optical microscopy

The blue-violet iridescent coloration covers the dorsal side of the legs segments closest to the cephalothorax, the "coxa", "trochanter" and "femur". The other segments ("patella", "tibia", "metatarsus" and "tarsus") are covered with dark brown setae, showing no iridescence. The first three of the six segments that form the pedipalp are also colored in a similar way. Traces of blue can additionally be seen on the chelicerae (those mouth parts used to grasp and crush food and to inject venom to paralyze prey) and at different places on the dorsal side of the cephalothorax (see Fig. 1(b)). Macrophotography and optical microscopy (see Fig. 1(c) and 1(d)) offer the advantage of color rendering and show that the blue coloration originates from special bristles covering the dorsal face of the spider's cuticle. This hairy region is covered with setae that are roughly parallel to each other and parallel to the cuticle's surface. Examination of the bristles under an (Olympus BX61) optical microscope, used in reflection mode, shows colors in the range of blue and violet. The blue coloration is most easily seen from a direction close to the normal to the cuticle surface. Under larger incidences or viewing angles, the coloration becomes violet and completely fades away with further angle increase. This iridescence suggests a structural coloration.

#183854 - $15.00 USD Received 22 Jan 2013; revised 23 Feb 2013; accepted 23 Feb 2013; published 13 Mar 2013

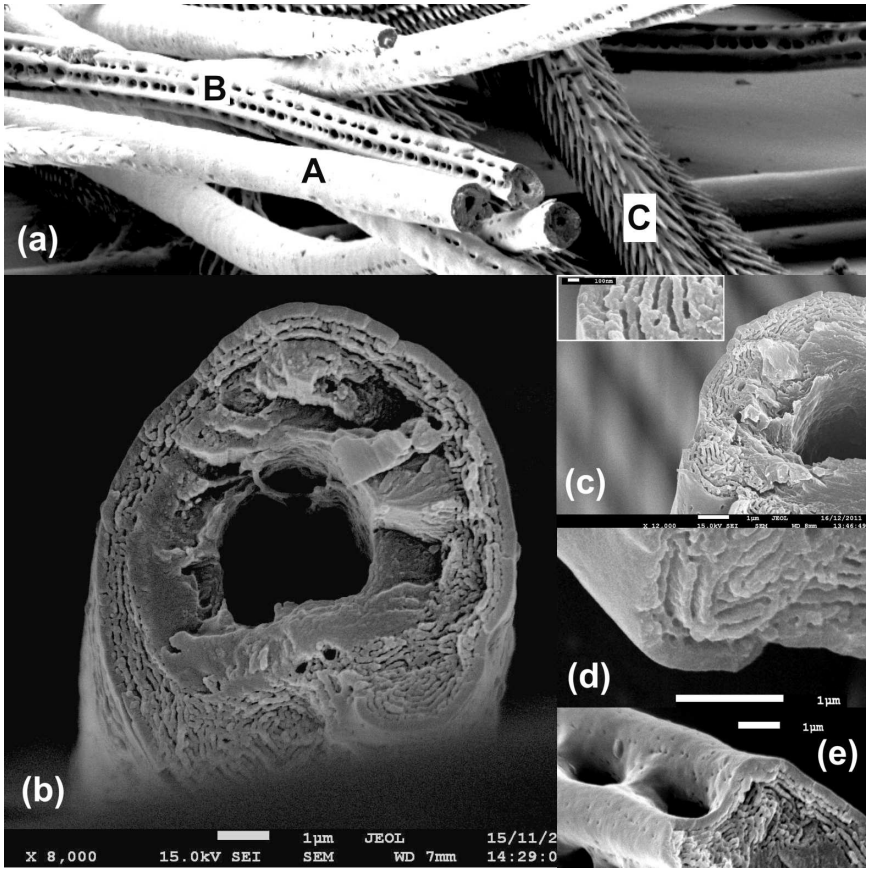

Fig. 2. (a) The different types of setae, as are revealed by scanning electron microscopy. Most of the setae are asymmetrical in cross section, with one side being cylindrical (A) and the other side flattened and sculpted (B) in a way that recalls the standard ridge-crossrib structure displayed by relatively unspecialized scales in other arthropods. Bristle C shows the sharp extensions typical of an "urticating bristle", designed to penetrate soft surfaces and produce irritation. (b) The whole cross-section of a blue seta, showing the layered outer cortex that surrounds the structure, the thick homogeneous substrate and the cylindrical cavity, all of which are centered on the axis of the cylinder. (c) Detail of the multilayered structure : a few (around 4) cylindrical sheets are repeated radially. The insert shows details at a larger magnification which suggests that the space between the sheets is essentially empty. (d) On this fractured cross-section, some sheets are protruding in such a way as to show their outer surface. This image also suggests a solid/air interface. (e) This view of the perforated part of the bristle reveals that the multilayer is also present there, providing blue-to-violet iridescent coloration.

4. Submicron morphology

4.1. Cross-section by Scanning Electron Microscopy

Figure 2 provide information on the structure of the blue setae, as acquired from scanning electron microscopy. Samples were prepared by cross-sectioning a femur from a foreleg, creating a sharp surface perpendicular to its axis, while keeping all the bristles attached. The operation was conducted at the temperature of liquid nitrogen, low enough to harden the chitinous mate-

#183854 - $15.00 USD Received 22 Jan 2013; revised 23 Feb 2013; accepted 23 Feb 2013; published 13 Mar 2013

rial and increase the chances of a neat fracture of the setae. The femur's segment was mounted flat or upright, using silver paint, on a metallic sample holder for viewing the setae's lateral surface and cross section as clearly as possible. The whole mounts were coated in metal (20 nm of gold) in order to ease charge elimination and then introduced in a JEOL 7500F high-resolution field-emission scanning electron microscope. About two dozen fractured cross-sections could be examined in this way.

Figure 2(a) provides a low-magnification view of the setae. On seta labeled A, the exposed surface is clearly a cylinder, but the presence of a more structured side appears on the fractured cross-section. The seta labeled B is just the same as seta A but turned over, so that it clearly shows the non-cylindrical region. Indeed, the cross section of this seta is similar to that observed on seta A, with a large angle of rotation. The bristle labeled C is much more complex, with barbs pointing backwards. Their oriented geometry suggests that the function of this structure is to penetrate soft surfaces under random motions: a mechanism cited for the urticating bristles. This view indicates that the bristles responsible for the coloration (A and B) can only be approximately described as cylindrical. The whole seta can be viewed as a long strip of chitinous material curved cylindrically perpendicular to the longitudinal direction and closed by a narrow net of "ribs" and "crossribs". Note that these characteristics make these specific setae rather similar to the appendages found in other arthropods, such as butterflies scales [7]. This complexity suggests multiple functionalities.

Figure 2(b) shows a nearly complete cross-section. The region near the center of the apparent structure, on the fiber axis, is hollow (making the whole bristle topologically akin to some kind of sack), while the outer part is a clearly distinguishable cortex, structured as a quasi-cylindrical multilayer and terminated by a thick protective layer. Between the outer multilayer and the inner cavity, the volume of material appears to be essentially homogeneous. Under grazing incidence and at grazing viewing directions, the bristles on the cuticle assume a dark brown coloration. Consequently it can be inferred that this bulk chitinous material contains many absorbing pigments (the coloration suggests melanin).

As seen in Fig. 2(b) and 2(c), the cylindrical multilayer has three or more "bilayer" periods (146 ± 10 nm for each period). Each period is formed by a layer of a high secondary electron emitter, which we assume to be a hard chitinous compound ("sheets" 100 ± 15 nm thick) and a layer which appears very dark and unstructured, that we identify as essentially empty (46 ± 15 nm). Bridges across this empty layer, between sheets, are frequently seen in high magnification conditions (see the inset in Fig. 2(c) and in Fig. 2(d)). These material bridges, which would not be needed if any another solid material was filling the space, contribute to rigidify the structure while acting as spacers. In fact, each chitinous sheet that form the solid/void cylindrical multilayer is itself structured in the tangential directions, but without affecting strongly the optical properties: we will come back to this in a moment. Note, also, that the outer cylindrical chitinous sheet is slightly thicker than the internal layers: 220 ± 20 nm of bulk chitin-based material.

Figure 2(d) shows several sheets of chitin, broken at different distances along the bristle's axis and protruding in such a way that their outer lateral surface becomes visible. This, and the bridges between adjacent sheets, suggest that they are separated by an empty layer. Figure 2(e) shows that, in the region of the ribs and cross-ribs, the same multilayer structure is also present, near the surface and deeper, but that the orientation of the layers is more turbulent than in the cylindrical part of the bristle.

The cylindrical multilayer is, as will be confirmed below, the origin of the blue coloration. In planar - not cylindrical - geometry, similar or more complex layered structures have been shown to be responsible for coloration of other arthropods (see specifically [8, 9], reviews in [10–14] and special multilayers in [15–17]). Iridescence is an important aspect of the optical properties

#183854 - $15.00 USD Received 22 Jan 2013; revised 23 Feb 2013; accepted 23 Feb 2013; published 13 Mar 2013

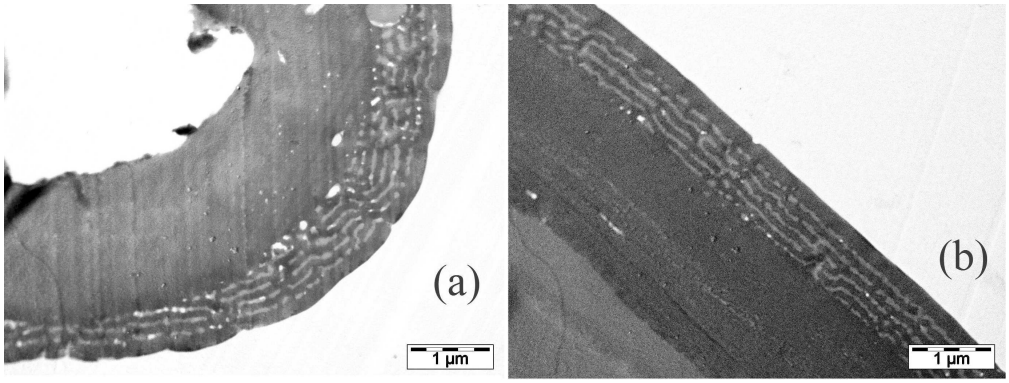

Fig. 3. Sections of the blue setae, viewed with the transmission electron microscope (TEM). The peripheral multilayer as seen (a) through a section at right angle from the seta axis and (b) through a section nearly parallel to the axis. The measurement of the multilayer period on these sections confirm the values obtained from scanning electron microscopy images. The slight opacity of the lighter layers is interpreted as the presence of infiltrated embedding medium between the darker cylindrical chitin sheets.

of these planar structure, which has its counterpart – slightly more complicated, see below, – in the case of a curved, cylindrical, surface.

4.2. Bristle's cross-section, as observed in Transmission Electron Microscopy

The SEM observations and data are confirmed by transmission electron microscope (TEM) images. However, as we will now see, some details call for caution and a careful discussion.

Samples were prepared by embedding individual bristles in an epoxy resin, letting this resin infiltrate the structure at a constant temperature of 35°C for 48 hours, and polymerize at 60°C for 72 more hours. Then, slices (90 nm thick) were cut perpendicular to the bristle's axis and examined with a FEI Tecnai Transmission Electron Microscope (TEM). Two typical images are shown in Fig. 3. Figure 3(a) shows the structure of the multilayer in the plane of the bristle-cross-section. Figure 3(b) gives a view of the same multilayer, along a section nearly parallel to the bristle's axis. The examination of these views confirms that: (1) The bristle is hollow; (2) The internal hollow cylindrical volume is homogeneous; (3) A thin cylindrical multilayer (3 or more bilayers) lies below the external surface; (4) The outer layer is thicker than those in the multilayer.

The interesting part is the multilayer, which shows alternate clear and dark layers. There is little doubt that the dark layers are made of the same chitinous material as the outer protective cortex and the internal hollow homogeneous cylinder: the electron opacity is the same. In the multilayer, the opacity of the "clear" layers separating the dark chitinous lamellae is not exactly the same as the opacity of the resin outside the bristle. This may suggest that the outer resin is different from the material imbedded between the dark sheets and the question of the nature of the interstitial material in the structure rises. Since SEM shows unambiguously that the spaces between chitin sheets are empty in the dry, non-embedded structure, we interpret the different opacities by assuming that, in the transport process into the multilayer's void spaces or during the long polymerizing time, the infiltrated resin has gathered some absorbing material and slightly changed its contrast with respect to the pure, outer-lying resin. This unwanted staining is likely to be difficult to avoid when treating a complex structure that has been preserved dry.

#183854 - $15.00 USD Received 22 Jan 2013; revised 23 Feb 2013; accepted 23 Feb 2013; published 13 Mar 2013

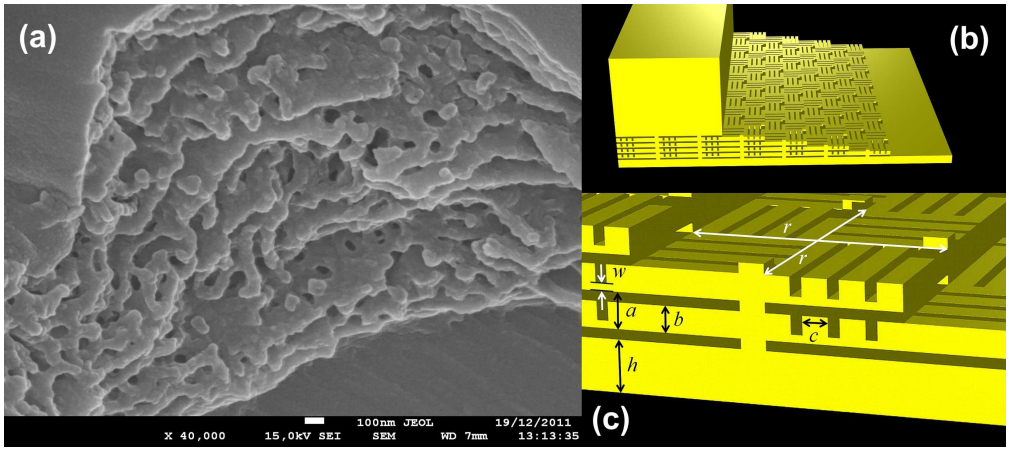

Fig. 4. (a) The bristle coloring structure, viewed through a window-like perforation on the cylinder's surface. The outer surface of the concentric layers is smooth except for random perforations. However, the edges of the sheets are highly structured, laterally, suggesting that the smooth surface hides a fine pattern of hard rods separated by air gaps. (b) An idealized model of the photonic structure suggested by SEM and TEM, with a thick covering layer, a multilayer build from winding chitin rods lying under a thin chitin sheet with binding bridges and a thick substrate. The structure is represented upside down (cover-layer below) in order to reveal the sheet patterning. This model neglects disorder and the cylindrical curvature. (c) The parameters that tune the optical properties of this ideal structure are as follows: h is the thickness of the cover layer, a is the total multilayer period, w is the thickness of the thin binding plate, b is the thickness of the chitin sheet, including the binding plate, c is the width of the chitin bars. r is an artificial lateral period for representing the pattern of rods in a square lattice symmetry.

4.3. Three-dimensional structure of the concentric sheets

In order to make more precise the structure of the chitin sheets, new samples were prepared for scanning electron microscopy by gluing individual colored bristles flat on conductive carbon adhesive tab on a metallic sample holder. A sharp blade was then used to puncture the bristles at many different places, providing many chances to damage the multilayer by removing outer sheets. A typical result is shown in Fig. 4(a). Several sheet surfaces are now apparent and the image shows that the sheets are themselves structured. The chitin sheet is built from flat, winding chitin bars that are separated by a roughly constant gap, hence the pattern observed on the sheet. The coherence and rigidity of this structure, reminiscent of those produced by spinodal phase separation [18], is enhanced by a thin, continuous lamella that attaches to one side of the flat chitin-bar assembly. When viewed from the outside of the bristle, this flat, cylindrical thin film is seen first, hiding the chitin-bar pattern, except at places where the supporting film is naturally or accidentally perforated. Again, from such images, it is clear that the dry structure has solid/air internal surfaces, and not solid/solid interfaces.

This photonic structure, formed from winded chitin rods on a thin continuous sheet, is only partially ordered: the distance between concentric sheets, the size of the cross-section of the chitin-rods and the gap that separates them are nearly constant. On a larger scale, the chitin bar pattern and the location of the bridges between the sheets are much more disordered. A possible (flattened and ordered) idealization of the whole structure is shown in Fig. 4(b). This structure is much more regular than the actual natural photonic structure, but, beyond accommodating the observed multilayer's characteristics, it introduces the structure of winded chitin bars on a very

#183854 - $15.00 USD Received 22 Jan 2013; revised 23 Feb 2013; accepted 23 Feb 2013; published 13 Mar 2013

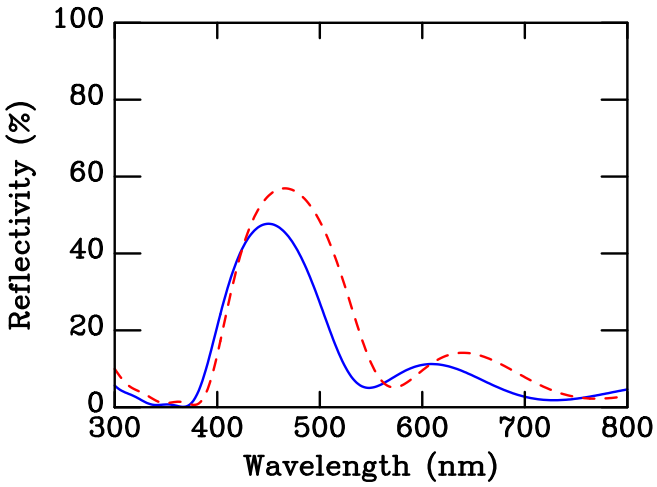

Fig. 5. Calculated reflection spectrum (solid line), based on the morphological data obtained by electron microscopy. The structure is the three-dimensional model described in Fig. 4(c). The dashed curve corresponds to the same calculation with all three-dimensional features – bridges between the sheets and the groove between the chitin bars – suppressed. In this case, the spectrum is exactly as one would expect from a one-dimensional multilayer. The red shift is consistent with the increase in the average refractive index.

thin continuous support. The size of the parameters which define this structure are extracted from the scanning and transmission electron microscopy data and summarized in Fig. 4(c). This three-dimensional structure will actually serves us to show that an even simpler structure – the cylindrical one-dimensional Bragg mirror – is, here, appropriate to model the reflection properties of the tarantula's bristles.

5. Reflection from a colored bristle

The cylindrical structure is actually a multi-scale system: the bristle diameter ($\approx$ 10 μm) defines a scale where optical phenomena are driven by incoherent ray-tracing optics, while, at the scale of the multilayer period ($\approx$ 150 nm), interference plays a major role. In the present work, we examine both scales independently.

5.1. Local reflecting structure

The ideal structure shown in Fig. 4(c) summarizes the observed shape and parameters that control the optical properties of the local reflector found on the spider's cylindrical bristles. The values of the parameters have been be extracted from the TEM and SEM images. Though these values may vary by as much as $\pm$10% on different images, the following values can be safely accepted: $h = 220$ nm is the thickness of the cover layer, $a = 146$ nm is the total multilayer period, $w = 26$ nm is the thickness of the thin binding plate, $b = 100$ nm is the thickness of the chitin sheet, including the binding plate, $c = 100$ nm is the width of the chitin bars. $r = 1000$ nm is an artificial lateral period for representing the pattern of rods in a square lattice symmetry replacing the isotropic irregular pattern. The exact value of the parameter r is deduced from the length of straight sections of the rods, when these can be detected. The homogeneous substrate layer has a thickness of about 2000 nm, but we will replace this with a semi-infinite medium. As the 2000 nm layer absorbs essentially all the transmitted radiation, this simplification has negligible consequences.

#183854 - $15.00 USD Received 22 Jan 2013; revised 23 Feb 2013; accepted 23 Feb 2013; published 13 Mar 2013

The refractive index of the solid part of the structure is that of chitin, with absorbing melanin. It is analogous to the dark chitin found in other arthropods. We use the value measured by Yoshioka *et al.* [19]. This measured value accounts for both dispersion and absorption: it varies from $n = 1.785 + i0.097$ at 400 nm to $n = 1.63 + i0.012$ at 700 nm. These values are higher than the commonly accepted average value, $n = 1.56 + i0.06$ [20], obtained for the clear chitinous compound in a Morpho butterfly scale. The real part of the refractive index may vary, in particular with the contents of the absorbing pigments, as indicated by Kramers-Kronig relations.

The three-dimensional transfer-matrix technique [21] can be used to calculate the specular reflectance from the structure shown in Fig. 4(b) (with 4 periods). The result, using a base set of 64 plane waves (which means 64 propagating and evanescent diffraction orders) is shown as a solid-line curve in Fig. 5. This calculation leads to a reflection band centered on the dominant wavelength 451 nm. Removing the bridges between the sheets and the groove between the chitin bars does not change the spectrum very significantly, as the dashed curve in Fig. 5 shows. The main reason for this agreement is that the three-dimensional features actually have little effect on the scattering of light: the bridges are small and weak scatterers, the gaps between the rods are too close to each other, compared to wavelength, to produce diffraction of visible waves. Neglecting the gaps between chitin rods, the bridges between chitin sheets and the overall cylindrical curvature, the coloring structure is a one-dimensional multilayer, or Bragg mirror.

This analysis shows that a one-dimensional Bragg mirror structure is highly justified and, from now on, we will use this much simpler, one-dimensional, representation of the structure.

Note that, in the context of a one-dimensional periodic multilayer, the reflected color can easily be predicted: the repetition of a bilayer, assembling a layer with a thickness $d_1 = b =$ 100 nm (refractive index averaged over the visible spectral range $n_1 = 1.73$) and an other one with a thickness $d_2 = a - b = 46$ nm (refractive index of air $n_2 = 1$) leads to the following dominant reflected wavelength

$$\lambda = \frac{2a\overline{n}}{m} \tag{1}$$

(see for instance Land [8] or Kinoshita *et al.* [22], who refer to the pioneering work of Lord Rayleigh in 1917 [23] (a simpler derivation, solely based on translational symmetry arguments, has been given by Vigneron *et al.* [21, 24]). In the above equation, m is an integer (at least equal to 1) that selects the band gap acting in the interesting range of wavelengths. Most often, in natural photonic structures, the value $m = 1$ is adequate, but exceptions have been found. The average refractive index mentioned by most authors is [22]

$$\overline{n} = \frac{n_1 d_1 + n_2 d_2}{d_1 + d_2} \tag{2}$$

where, here, $d_1 + d_2 = a$. Another way of approaching $\overline{n}$ is to average the dielectric constant $\overline{\varepsilon}$ [21, 24] and then deduce the average refractive index, but for moderate refractive indexes, both procedures lead to very similar results. Here, from Eq. (2), $\overline{n} = 1.50$ ($\sqrt{\overline{\varepsilon}} = 1.54$) so that the dominant reflected wavelength is $\lambda = 438$ nm (from $\overline{\varepsilon}$: 450 nm) – very close to the maximum reflection wavelength on the spectra in Fig. 5. This wavelength indicates a purplish blue color [25]. This very simple approach (1) assumes an infinite stack, (2) neglects the special outer layer and (3) neglects absorption by dark pigments. More importantly, the cylindrical curvature of the multilayer is not yet accounted for. This is the object of the next section.

5.2. Scattering from a cylindrical reflecting structure

The scattering by structured and unstructured cylinders have been considered in the context of optics and radio-wave propagation [26–28]. It is interesting to note that one of the first

#183854 - $15.00 USD Received 22 Jan 2013; revised 23 Feb 2013; accepted 23 Feb 2013; published 13 Mar 2013

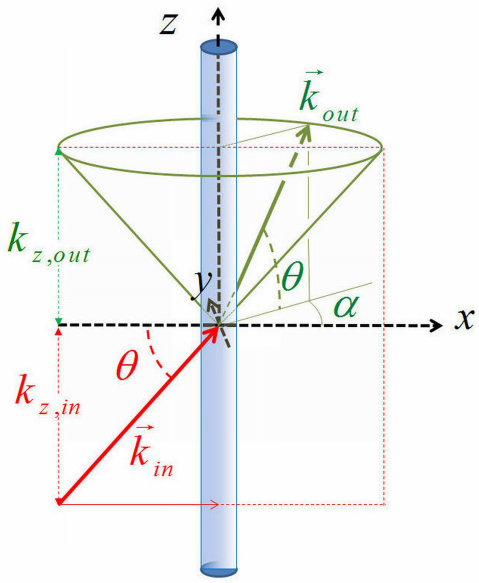

Fig. 6. The model's geometry. The cylindrical fiber is set along the z axis (which is also the cylinder's axis) and the incident beam (along $\vec{k}_{in}$) lies in the plane containing the x axis. Due to conservation laws, the scattered beam (along $\vec{k}_{out}$) lies on the surface of a cone and makes the same angle to the xy plane as the incident beam. Once the incidence angle θ is set, the possible emergent directions are described by a single parameter, the azimuthal angle α.

applications of the theory of cylindrical light scattering was dealing with spider web fibers [29]. As seen in the past history of this problem, the full vectorial treatment of the scattering by a cylinder is a rather cumbersome calculation, which requires the solution of Maxwell's equations for cylindrical coordinates. This calculation is interesting and important because it is amenable to the quantitative numerical evaluation of the directional scattering spectra. In the present case, we only need to provide a short account of this question, relevant to the present study.

The approach is inherently multiscale, considering that the radius of the cylinder is large compared with the incident radiation wavelength. This is clearly the case here, where the diameter of the seta is of the order of 10 μm, while the optical layers found in the cortex are only about 150 nm thick. This allows to treat the global illumination of the bristle from the point of view of geometrical optics, while the scattering on the light ray on the cylinder surface is treated with the prescriptions of wave optics. There, all the details introduced by Maxwell's equation on a multilayer optical filter are accounted for. This type of two-scales approach was used, for instance, when discussing the iridescence of the shield bug *Calidea panaethiopica* [30] and, since then, in a number of other occasions.

Figure 6 shows the geometry of the scattering problem. An infinitely long cylinder is set upright, along the z axis. Its surface with air is structured by the presence of a multilayer, while the volume, below the multilayer, is a homogeneous, strongly absorbing, material. The incidence plane contains the incidence beam (with wavevector $\vec{k}_{in}$ and the cylindrical fiber's axis. This plane defines the x cartesian axis, so that the incident wave vector has no y component.

The output wave vector $\vec{k}_{out}$ is constrained by two invariance prescriptions:

1. The frequency of the incident wave ω is conserved, because the medium dielectric re-

#183854 - $15.00 USD Received 22 Jan 2013; revised 23 Feb 2013; accepted 23 Feb 2013; published 13 Mar 2013

sponse has no time dependance. This means that the norm of the output wavevector, $k_{out} = \omega/c$ is identical to that defined by the input wavevector. The end of the output wave vector $\vec{k}_{out}$ is found on the surface of a sphere of radius ω/c, centered on the origin.

2. The z component k_z of the wave vector is also conserved because the propagating medium has full translational invariance in the direction of the cylinder axis. The z component of the output wave vector must be identical to the z component of the input wave vector. Following this, the output wave vector must point somewhere on the horizontal plane (parallel to xy) at $z = k_{z,in}$.

This plane intersects the sphere of constant frequency along an horizontal circle centered on the cylinder axis. This means that, when a beam of light strikes a cylindrical fiber from any incidence, the scattered light escapes along the surface of a cone with the same axis as the cylinder. The angle from the fibre axis to $\vec{k}_{out}$ is the same as the angle from the fibre axis to $\vec{k}_{in}$. This statistical redirection of an incident beam about the axis of the fiber, in the cone described here, was recognized, some years ago, as a new mechanism for guiding waves in biological fibrous materials, such as dentin [31].

This result – namely the distribution of the scattered waves on the periphery of a cone of known opening angle – results only from exact conservation laws, so that it is valid for any applicable fiber diameter and light wavelength. It is a robust result in the context of wave optics, as well as ray-tracing optics. For fiber radii significantly larger than the incident light wavelength, there is an instructive interpretation of this result (from ray-tracing optics) which helps with understanding the expected optical behavior of the fiber.

The incident wave vector has cartesian coordinates

$$\vec{k}_{in} = \frac{\omega}{c}(\cos\theta, 0, \sin\theta) \tag{3}$$

where the angle θ is the angle between the incident beam and the xy plane, at a right angle to the fiber axis (see again Fig. 6). θ is also the angle between any outgoing wave vector $\vec{k}_{out}$ and

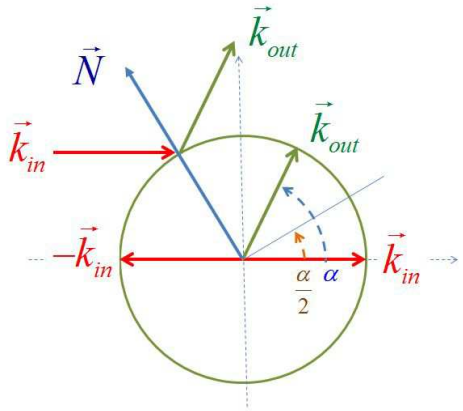

Fig. 7. The projection of the elements of Fig. 6 in the xy plane, showing the direction of the vector $\vec{N}$ bisecting the angle between $-\vec{k}_{in}$ and $\vec{k}_{out}$. This shows that the scattering by the fiber, under the invariance conditions which conserve the norm and the z component of the wave vector, can be seen as a reflection on the fiber surface, from the point where this surface meets the normal $\vec{N}$.

#183854 - $15.00 USD Received 22 Jan 2013; revised 23 Feb 2013; accepted 23 Feb 2013; published 13 Mar 2013

the *xy* plane. There is only one parameter which fixes the direction of the outgoing wave $\vec{k}_{out}$, namely its azimuthal angle α, measured from the *x* axis:

$$\vec{k}_{out} = \frac{\omega}{c}(\cos\theta\cos\alpha, \cos\theta\sin\alpha, \sin\theta) \tag{4}$$

The whole circle is described for $0 \leq \alpha < 2\pi$. In particular, $\alpha = 0$ corresponds to $\vec{k}_{out} = \vec{k}_{in}$ and a "straight through" ray trajectory. The "longitudinal" reflection on the fiber axis, in the incident *xz* plane, gives an outgoing wave vector with $\alpha = \pi$.

The angle 2δ between the incident beam and the emergent beam can be calculated from the scalar product

$$\cos 2\delta = \frac{(-\vec{k}_{in}) \cdot \vec{k}_{out}}{(\frac{\omega}{c})^2}. \tag{5}$$

This leads to the following value of half the angle between the "in" and "out" beams,

$$\cos\delta = \cos\theta \sin\left(\frac{\alpha}{2}\right) \tag{6}$$

Now, the vectors $\vec{k}_{in}$ and $\vec{k}_{out}$, together, define a plane that does not (in general) contain the fiber axis. If we look for the vector that bisects the angle between $(-\vec{k}_{in})$ and $\vec{k}_{out}$, we find the vector $\vec{N}$ which lies in the *xy* plane:

$$\vec{N} = (-\sin\left(\frac{\alpha}{2}\right), \cos\left(\frac{\alpha}{2}\right), 0) \tag{7}$$

This direction is visualized in Fig. 7, which shows the relevant vectors projected onto the *xy* plane. The vector $\vec{N}$ is always normal to the fiber axis (so in the *xy* plane). It is constructed as the perpendicular to the fiber radius at an angle $\alpha/2$ from the *x* axis. This normal is in the plane defined by the "in" and "out" beams and these beams both make the same angle δ with this normal. The scattering of the incident beam on the fiber, from $\vec{k}_{in}$ to $\vec{k}_{out}$, can then be interpreted, in three dimensions, as a reflection of a light ray which hits the cylinder surface at the intersection point with the direction of the normal $\vec{N}$.

This result allows to determine the color scattered along the cone surface, at the azimuth α, when the cylinder surface is covered by a cylindrical Bragg mirror. The angle of incidence δ for the reflection is given as a function of the azimuth by Eq. (6) and the dominant wavelength in this direction is approximately (i.e. under the assumption – as justified above – of a "local" infinite planar multilayer [24, 32]

$$\lambda = \frac{2a\sqrt{\bar{\varepsilon} - 1 + \sin^2(\frac{\alpha}{2})\cos^2\theta}}{m} \tag{8}$$

Figure 8 shows the iridescence produced by the absorbing Bragg mirror described above, curved to form a cylinder and evaluated according to Eq. (8). We note that the curves indicate an iridescence that locate the dominant wavelength between blue (450 nm) and near-ultraviolet (342 nm). The maximal iridescence richness [33] is obtained when $\alpha = 180°$, a geometry for a longitudinal reflection on the fiber surface, when the incident beam, the reflected beam and the fiber axis are all in the same plane. The other extreme case, $\alpha = 0°$, corresponds to a straight, tangential, transit of the light, in the *xz* plane, without any direction change. In this situation, the local incidence angle on the surface approaches 90°, with an impact parameter (distance to the fiber's axis) equal to the fiber radius, so that the reflected wavelength experiences a maximal shift to the ultraviolet. This grazing reflection occurs for any value of the incidence on the fiber

#183854 - $15.00 USD Received 22 Jan 2013; revised 23 Feb 2013; accepted 23 Feb 2013; published 13 Mar 2013

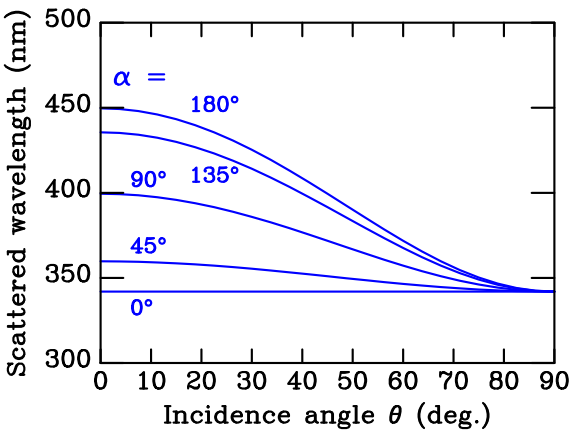

Fig. 8. Dominant fundamental scattered wavelength, for various values of the incidence angle θ, measured from the *xy* plane, normal to the fiber, and for various azimuthal directions α of the scattered beam in the outgoing wave cone. The iridescence (change of color with viewing direction is maximal for a full reflection in the longitudinal direction of the fiber ($\alpha = 180°$) and minimal for a tangential, grazing transit ($\alpha = 0°$). For parameters matching those of the multilayer found on *Pamphobeteus antinous*, the scattered wavelengths span a blue-to-ultraviolet range.

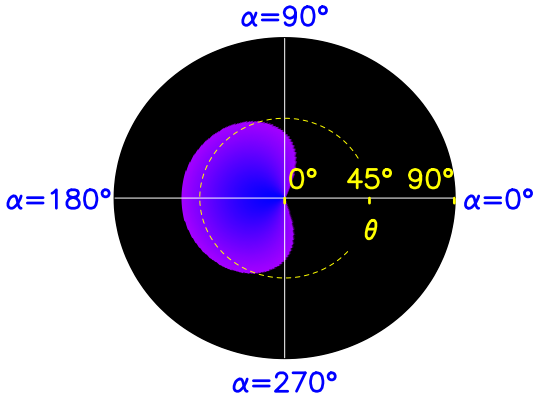

Fig. 9. Polar plot of the cylindrical Bragg mirror iridescence. The outgoing wave direction is determined by the angle θ to the *xy* plane (the same as for the incident wave) and the azimuthal angle α. The black area corresponds to the direction where, for humans, no coloration occurs, because the scattered wavelength is ultraviolet, below 380 nm. The lighter shades area indicate visible light, blue in the central region and violet near the border. The plot is based on Eq. (8).

(the angle θ), so that the reflected wavelength is constant, the spectral richness vanishes, and the wavelengths become degenerated.

Another important remark relating to the result brought by this model is that the human access to colors is restricted to wavelengths larger than 380 nm, so that the range of visibility is limited, for both angles θ and α. Figure 9 essentially provides the same information as Fig. 8 and Eq. (8), but indicates (in black) (α, θ) areas of the polar plot where the emission is invisible to humans, because it is shifted into the ultraviolet range.

#183854 - $15.00 USD Received 22 Jan 2013; revised 23 Feb 2013; accepted 23 Feb 2013; published 13 Mar 2013

6. Spectrophotometric measurements

The above theoretical considerations suggest optical experiments. Spectrophotometric hemispheric measurements were first performed with a double-beam spectrophotometer Perkin Elmer Lambda 750S. This apparatus is equipped with an integrating sphere and pre-aligned tungsten-halogen and deuterium sources, covering the UV-visible and the near-infrared spectral regions. The measured reflectance is normalized to the diffuse reflection of a polytetrafluoroethylene calibrated standard. For this experiment, the blue side of a whole femur from the spider's leg was exposed to a parallel light beam under near-normal incidence. The spot was a rectangle 1 cm high (along the femur long dimension) and 0.5 cm wide (within the width of the femur). The measurement included diffuse scattering from all kinds of bristles on the probed surface, as well as from the flat integument that supports these bristles.

Figure 10 shows the result of this hemispheric reflectance measurement for an incident beam normal to the cuticle. This reflection shows a broad enhancement close to 430 nm, with a bandwidth approximately equal to 100 nm (FWHM). This band induces a perception of purplish blue, not so far from the end of the human visible spectrum. The reflectance also increases towards the red. This broad reddish contribution can also be seen on non-iridescent parts of the spider's body, so that it is interpreted as originating from the scattering properties of dark pigments. Many of the pigments on the spider's cuticle, indeed, tend to absorb short-wavelength radiation and to scatter long wavelengths, in the red and infrared.

An Avaspec 2048/2 fiber-optic spectrometer was used for fixed-angle specular measurements. The measurement chain was equipped with a combined equilibrated halogen-deuterium source covering 250 nm - 1100 nm, slightly exceeding the human visible spectral range. In these measurements, the intensity is also systematically compared with the intensity of light scattered by a standard, diffusive white, polytetrafluoroethylene reference surface, under identical angular configurations. With this normalization, the reflected intensity is usually referred to as a "reflection factor," expressed in %. This quantity is not bound to be less than 100%. The optic fiber that brings the illumination in, and the fiber that takes the reflected signal out, are equipped with ferules 1.5 mm in diameter, so that the measurement takes place in a circular area of 2 mm, again incoherently collecting the light from several blue bristles (approximately parallel to each other) and from the flat integument, deeper.

The structural origin of the blue coloration leads to the phenomenon of iridescence, which

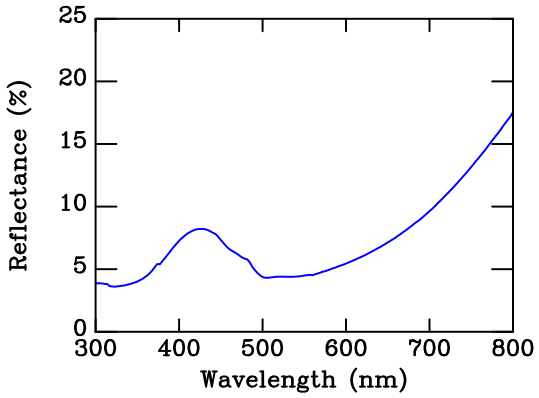

Fig. 10. Measured hemispheric reflectance spectrum of a blue area on the spider's cuticle, under near normal incidence. The distribution of reflected wavelengths peak near 430 nm, due to iridescence. This spectrum integrates contributions from all outgoing directions.

#183854 - $15.00 USD Received 22 Jan 2013; revised 23 Feb 2013; accepted 23 Feb 2013; published 13 Mar 2013

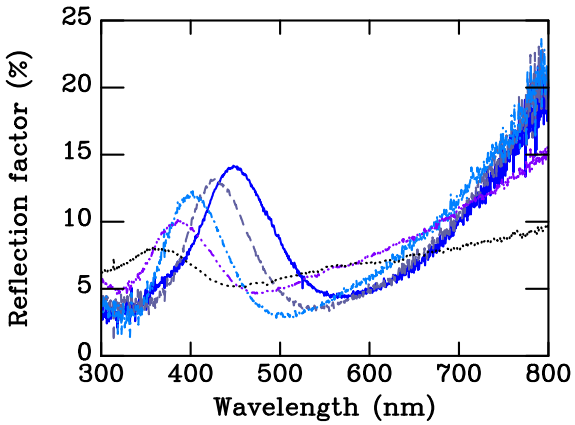

Fig. 11. Iridescence of the "blue" setae of the spider *Pamphobeteus antinous*. The wavelength selected by the cylindrical Bragg mirror experience a blue shift when the incidence angle (measured from the normal to the fiber) is increased. The spectra reported are obtained in a longitudinal specular reflection geometry $\alpha = 180°$. Solid line: $\theta = 15°$; dashed: $\theta = 30°$; dot-dash: $\theta = 45°$; dot-dot-dot-dash: $\theta = 60°$; dotted: $\theta = 75°$.

– here – depends on both the incidence (θ) and the outgoing azimuthal angles (α). Figure 11 shows the spectra measured for the special direction $\alpha = 180°$, for which the iridescence richness is maximal.

These measurements confirm that the dominant reflected wavelength shifts to shorter wavelengths as the incidence angle is increased. The color changes from purplish blue to deep violet and ultraviolet. However, the intensity and saturation of the reflected light fades away as the wavelength approaches ultraviolet. Since a multilayer response would not explain this fast decrease in intensity, we suggest that short-wavelength absorption takes place in the chitinous materials that constitutes the optical structure. In the present case, the black region in Fig. 9, due to a shift to invisible radiation, is also a region of low scattering intensity. The limitation of the reflection does not imply a correlated absence of visual sensitivity: spiders do perceive ultraviolet radiation [34].

The spectral bandwidth of the spectra shown in Fig. 11 is much larger than could be expected from the gap width implied by the relatively weak refractive index differences that are characteristic of natural structures. The reason for the broadening could have been disorder, but this turns out not to be the case: the axes of the setae fluctuate about the long direction of the spider's femur, but not by much more than about 10° and optical microscopy inspection shows that most of the setae present their cylindrical side outwards, so that the hidden irregularities do not influence the optical response very significantly. The coloring function of the cylindrical Bragg mirrors remains rather robust in presence of this kind of disorder. In fact, the origin of the broadening can be better understood by considering the very limited number of layers and the strong absorption by the chitinous compound that constitutes the bristle.

A spectrum calculation, based on the above model – a "local" multilayer consisting of a 220 nm black chitin cover layer supporting four bilayers (46 nm air and 100 nm black chitin) on a thick dark chitin substrate and an incidence angle δ given by Eq. (6) as a function of θ and α – confirms the location and blue shift of the "purplish blue" iridescence and the origin of the broadening. The spectra in Fig. 12, computed for $\alpha = 180$ (this corresponds to the measurements setup for Fig. 11) are presented for the same five values of the incidence angle θ. The bandwidth and the iridescence of the calculated coloration band are consistent with the values

#183854 - $15.00 USD Received 22 Jan 2013; revised 23 Feb 2013; accepted 23 Feb 2013; published 13 Mar 2013

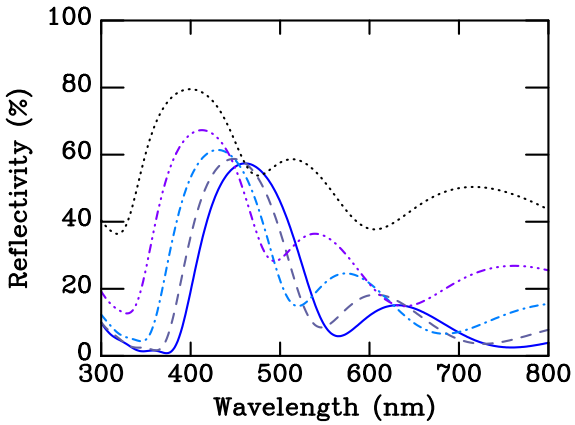

Fig. 12. Calculation of the unpolarized reflectance spectrum of a perfect multilayer mirror, avoiding all effects of disorder, for a longitudinal specular reflection geometry, under conditions similar to those in Fig. 11. Solid line: $\theta = 15^\circ$; dashed: $\theta = 30^\circ$; dot-dash: $\theta = 45^\circ$; dot-dot-dot-dash: $\theta = 60^\circ$; dotted: $\theta = 75^\circ$. The structure is assumed flat, with a 220 nm black chitin cover layer above four bilayers (46 nm air and 100 nm black chitin) and a thick black chitin substrate. Black chitin is absorbent and dispersive [19]. Note that the calculated reflectivity is normalized by the incident intensity, while the reflection factor in Fig. 11 is normalized by the diffuse reflection from a white PTFE standard.

observed in the measured reflection factor. This suggests that the consideration of disordered effects should not add much to the spectral width, due to the limited thickness and due to the role of its contents in absorbing melanin. Note, however some discrepancies exist: the rise in the reflectance for long wavelength and the weakening of the constant background reflection at large angles are not reproduced satisfactorily by the model. These features may be controlled by unidentified pigments that are not accounted for in the simulations.

7. Conclusion

The setae which cover the dorsal side of the femurs and other parts of the cuticle of a mature male tarantula *Pamphobeteus antinous* are colored by a cylindrical Bragg mirror.

In nature, a few bristles and other kind of fibers have been observed to be brightly colored. Certain Polychaete worms, for instance [35, 36], have evolved bristles structured as two-dimensional photonic crystals. The marine worm *Aphrodita aculeata* has rigid spines and flexible bristles shaped as hollow tubes, with walls containing a two-dimensional triangular array of straight, parallel, microchannels. These bristles are produced by the secretion of chitin and protein from the base of cylindrical "microvilli"; the microvilli then leave the empty microchannels, as new material is extruded from their sides. The way the structure shown in the present study is produced may be quite different, as the bristles show many similarities with standard arthropod scales, some of which assume the shape of cylindrical rods [37, 38]. The highly structured part of the setae is, indeed, strongly reminiscent of a standard ridge-crossrib structure. An examination of how complex structures can vary between close species can be found in Ghiradella and Butler [39] and a review of the formation of this type of complex structural appendages can be found in Ghiradella [7]. Ideas on how living organisms actually produce these complex photonic structures are very important, as the structural coloration of fibers may avoid many of the difficulties encountered in the deposition of stain on textile fibers.

Meanwhile, from a biomimetic point of view, we can see potential for artificial ways of

#183854 - $15.00 USD Received 22 Jan 2013; revised 23 Feb 2013; accepted 23 Feb 2013; published 13 Mar 2013

obtaining fibers coated with a Bragg mirror that produces a structural coloration. Efforts have already been made towards that end, mostly for planar surfaces [14, 40, 41] or more elaborate hybrid structures [42].

Designing structurally colored fibers is a very active field, as fibers with coloration are useful in fabrics for clothes, papers, paints, etc... Structurally colored fibers using polymers (polyethyleneterephtalate with refractive index 1.63 and nylon-6 with refractive index 1.53) have been described by Hiroshi Tabata [43], who also consider some of their potential applications. The type of fibers described there are shaped as a long and narrow strip: a strongly anisotropic geometry. The cylindrical invariance discussed here may present advantages when considering knitting fibers to produce fabrics with large surfaces. Closer, but still not identical to the structure inspired by *Pamphobeteus antinous* is the recent demonstration, by Finlayson et al. [44] of an extruded polymeric opal fiber that is knittable and shows strong structural colors, that are tunable by applying mechanical tension.

Structurally colored fibres owe their importance, partly, to difficulties with the use of pigments. Although pigments have been used for many centuries to dye fabrics, this is a particularly polluting process because of the requirement for preconditioning the fibres and their limited capacity for absorbing dyes. This has long been known, for instance for vegetable dyes on wool or, more recently, for synthetic dyes on synthetic fabrics. Using structural coloration on textile materials – as in the colored fibers used by the tarantula *Pamphobeteus antinous* – may open an important way of developing textile colors, with the supplementary advantage of offering a wide range of new visual effects, due to iridescence and a tunable level of disorder.

Acknowledgments

P. S. acknowledges the Wallonia-Brussels Federation for financial support. A. B. was supported as a PhD student by the Belgian Fund for Industrial and Agricultural Research (FRIA). J.-F. C. is supported by the F.R.S.-FNRS (BELGIUM) as Research Associate. The project was partly funded by the Action de Recherche Concertée (ARC) Grant No. 10/15-033 from the French Community of Belgium. The authors also acknowledge using resources from the Interuniversity Scientific Computing Facility located at the University of Namur, Belgium, which is supported by the F.R.S.-FNRS under convention No. 2.4617.07.

#183854 - $15.00 USD Received 22 Jan 2013; revised 23 Feb 2013; accepted 23 Feb 2013; published 13 Mar 2013